Remote Sensing of Environment 113 (2009) 137–147

Contents lists available at ScienceDirect

Remote Sensing of Environment

journal homepage: www.elsevier.com/locate/rse

# Satellite-driven modelling of Net Primary Productivity (NPP): Theoretical analysis

Ana Prieto-Blanco [a,b,*], Peter R.J. North [a,b], Michael J. Barnsley [a,b,1], Nigel Fox [b]

[a] NERC CLASSIC, University of Wales, Swansea, UK
[b] Department of Geography, University of Wales, Swansea, UK
[c] National Physical Laboratory, Teddington, Middlesex, UK

ARTICLE INFO

*Article history:*
Received 19 February 2007
Received in revised form 1 September 2008
Accepted 6 September 2008

*Keywords:*
NPP
LAI
Hyperspectral
Ecological models
MISR

ABSTRACT

Ecological models are central to understanding the global hydrological and carbon cycles, and need data from Earth Observation to function effectively at regional to global scales. Here, we develop and apply an end-to-end analysis that relates the requirements of ecological models to the capabilities of satellite-sensors, starting with radiometric noise at the instrument, which collects the information, running through to the error on the estimated NPP output from the ecological model. In the process, the input requirements of current ecological models are reviewed. Our aim is to establish a better informed framework for the design and development of future satellite-sensor missions, which meet the needs of ecological modellers. Three mathematical models (PROSPECT, FLIGHT and 6S) are coupled and inverted using a technique based on LUT. The LUT are used to estimate biophysical variables of vegetation canopies from remotely-sensed data observed at the TOA in a number of viewing directions and in several wavebands within the visible and near-infrared spectrum. The five variables considered here are LAI, leaf chlorophyll content ($C_{ab}$), fAPAR, cover fraction and AOT. Different sensor configurations are investigated, in terms of directional and spectral sampling. The retrieval uncertainty is linked with the instrument radiometric accuracy by analysing the impact of different levels of radiometric noise. The parameters retrieved via the inversion are used to drive two LSP models, namely Biome-BGC and JULES. The effects of different sensor configurations and levels of radiometric noise on the NPP estimated are analysed. The system is used to evaluate the sensor characteristics best suited to drive models of boreal forest productivity. The results show that multiangular information improves dramatically the accuracy with which forest canopy properties are estimated. Due to problems of equifinality, the results show a persistence of error even in the presence of zero noise from the sensor, although decreasing the level of radiometric noise from 0.02 to 0.001 reduces error in the estimated NPP by 10% to 25%.

© 2008 Elsevier Inc. All rights reserved.

## 1. Introduction

Diagnosis and prediction of climatic, environmental and ecological changes in the Earth system is an enormously challenging task (IPCC, 2001, 2007). Better understanding of the processes involved, including those relating to Earth's radiation budget, atmospheric aerosol transport, vegetation and climate interactions, and carbon cycle, is required to address issues ranging from climatic change to environmental degradation. Ecological studies have traditionally focused on in situ observations of specific species at individual sites. These observations must be applied across a range of scales to address the needs of regional and global studies and to provide the broader insight needed of the entire Earth system. Ecological and climatic models allow us to extrapolate the physical processes, such as photosynthesis, respiration and evapotranspiration, which are measured at the leaf and canopy scale, to larger regions and longer temporal scales. Models are, therefore, a fundamental tool and their requirements an important input to the design of future satellite-sensor missions.

### 1.1. Requirements for biophysical parameters

Land-surface process (LSP) models describe the physiological and biophysical processes of soil and vegetation, including ecosystem Net Primary Productivity (NPP). Models of this type have assumed greater importance in recent years, and are now commonly incorporated to global climate models (Cox et al., 1999; Cramer et al., 2001). Land-surface process (LSP) models are also analysed in their own right to understand better the global carbon cycle (Kimball et al., 1997a,b; Potter et al., 2003). LSP models require information on a number of land-surface properties (e.g., land cover, leaf area index (LAI), roughness length and albedo), which are used to characterize the state of the land-surface and atmosphere system, in addition to meteorological data (e.g., daily values of maximum and minimum air temperature, total solar radiation, mean humidity and total precipitation). Satellite remote sensing can provide some of these inputs, and reference values to check the model outputs, at the required temporal and spatial scales (Chen et al., 2003; Lambin & Linderman 2006; Turner et al., 2006).

* Corresponding author. Department of Geography, University of Wales, Swansea, UK.
*E-mail address:* prieto@geog.ucl.ac.uk (A. Prieto-Blanco).
[1] Deceased.

0034-4257/$ – see front matter © 2008 Elsevier Inc. All rights reserved.
doi:10.1016/j.rse.2008.09.002

**Table 1**
Requirements for land-surface modelling

| | Source | Spatial resolution | Temporal resolution | Accuracy |
|---|---|---|---|---|
| Aerosol — total column | GCOS,GTOS | 1 km, 5 km | 24 h | – |
| | WMO | 50 km, 100 km | 0.25 h, 1 h | 10%, 10% |
| | IGBP | | 7 d | 10% |
| Albedo | Sellers et al. (1995) | 250 km | 30 d, 1 d, diurnal cycle | ±0.02 |
| Cloud imagery | GCOS, GTOS | 1 km | 3 h | – |
| Downwelling long-wave radiation at the Earth surface | GCOS, GTOS | 25 km | 3 h | ±5 W/m$^2$ |
| Downwelling short-wave radiation at the Earth surface | GCOS, GTOS | 25 km | 24 h | ±5 W/m$^2$ |
| Downwelling solar radiation at TOA | GCOS | – | 3 h | ±1 W/m$^2$ |
| Fire area/temperature | GCOS,GTOS | 0.1 km | 10 d | 5%/50 K |
| | IGBP | 3 km | 10 d | 5%/200 K |
| | UNEP | 0.5 km | 1 d | 5%/50 K |
| fAPAR | GCOS | 0.1 km | 10 d | 5% |
| | IGBP | 0.03 km, 50 km | 10 d | 5% |
| Land cover | WMO | 10 m, 100 m | 0.02 y, 1 y | 50 classes, 10 classes |
| | GCOS, GTOS | 100 m | 1 y | 50 classes |
| | IGBP | 30 m, 100 m, 1 km | 1 y | 22, 22, 2 classes |
| | UNEP | 1 m | 1 y | 20 classes |
| Land-surface imagery | GCOS, GTOS | 1 m | 4 y | – |
| | WMO | 10 m | 1 d | – |
| Land-surface topography | GCOS, GTOS | 10 m | 10 y | 30 (vert) |
| | WMO | 100 m | 10 y | 1 m (vert) |
| | IGBP | 10 m, 1 km | 100 y | 0.3 m, 1 m (vert) |
| LAI | GCOS, GTOS | 0.1 km | 10 d | 20% |
| | WMO | 0.01 km, 10 km, 50 km | 5 d, 7 d, 7 d | 5% |
| Land cover | GCOS | 0.1 km | 1 y | 50 classes |
| | WMO | 0.01 km, 0.1 km | 0.02 y, 1 y | 50, 10 classes |
| | IGBP | 0.03 km, 0.1 km, 1 km | 1 y | 22, 22 and 2 classes |
| | UNEP | 1 m | 1 y | 20 classes |
| Outgoing long-wave Earth surface | GCOS, GTOS | 25 km | 3 h | ±5 W/m$^2$ |
| Outgoing long-wave radiation at TOA | GCOS, GTOS | 50 km, 200 km | 20 d, 3 h | ±5 W/m$^2$ |
| | WMO | 0.1 km, 10 km, 50 km | 1 h, 0.5 h, 1 h | ±5 W/m$^2$ |
| | IGBP | 200 km | 6 h | ±10 W/m$^2$ |
| Ozone profile — total column | GCOS, GTOS | 1 km | 24 h | – |
| | WMOS | 10 km, 20 km, 25 km, 50 km | 0.5 h, 0.25 h, 6 h, 1 h | 5 DU (Dobson units) |
| PAR | Sellers et al. (1995) | 250 km | 30 d, 1 d, diurnal | ±10 W/m$^2$ |
| | WMO | 5 km | 1 h | 5% |
| Snow cover | GCOS, GTOS | 1 km, 100 km | 24 h | 5%, 10% |
| | WMO | 0.1 km, 1 km, 5 km, 15 km | 24 h, 120 h, 1 h 12 h | 5%, 2%, 10%, 10% |
| | WCRP | 1 km, 15 km | 24 h | 10% |
| Short-wave Earth surface bidirectional reflectance | Sellers et al. (1995) | 250 km | 30 d | ±10 W/m$^2$ |
| | WMO | 25 km | 24 h | ±5 W/m$^2$ |
| | IGBP | 100 km | 7 d | 1% |
| Vegetation type | WMO | 10 m, 50 m, 50 km | 7 d, 30 d, 7 d | 50, 30, 18 classes |
| | IGBP | 10 m, 100 m, 1 km | 10 d, 1 y, 90 d | 2, 18, 18 classes |
| | UNEP | 1 m | 1 y | 18 classes |

Only optimum values are shown.
Sources: ISLSCP Workshop (Sellers et al., 1995); Global Climate Observing System (GCOS); World Meteorological Organization (WMO); Global Terrestrial Observing System (GTOS); International Geosphere–Biosphere Programme (IGBP); World Climate Research Programme (WCRP); United Nations Environmental Program (UNEP). CEOS/WMO database, Observational requirements (WMO, WCRP, GCOS, GOOS, GTOS, IGBP, ICSU, UNEP).

Increasing availability of remotely-sensed data (Diner et al., 2005; Friedl et al., 2002) and growing interest in quantifying the terrestrial carbon flux (Canadell et al., 2003; IPCC, 2001) have driven forward research on the integration of LSP models and satellite remote sensing (Kimball et al., 1997a; Plummer 2000; Sellers et al., 1997a; Turner et al., 2004). The present tendency is toward "model–data synthesis" (Raupach et al., 2005), a combination of models and observations, which involves both parameter estimation and data assimilation techniques. In this approach, the uncertainties involved are as important as the parameter values. It is critical to define the requirements of LSP models from satellite remote sensing with a view to defining the characteristics of future satellite-sensor missions. Uncertainties associated with the parameters retrieved by remote sensing are hard to quantify as the ground truth measurements, where available, must be scaled up to larger areas to be compared with the satellite-sensor data (Heinsch et al., 2006; Morisette et al., 2002). Future satellite missions are now being designed taking into account the requirements of the users, often expressed as end-product specifications (Townshend and Justice 2002). These requirements are slowly being refined with input from the broad science community (Sellers et al., 1995, Townshend and Justice 2002, Table 1).

### *1.2. Retrieval of biophysical parameters from satellite observations*

Many biophysical data sets, notably those derived from long-term NOAA/AVHRR observations, are derived empirically from spectral reflectance measurements, using so-called vegetation indices such as the normalized difference vegetation index (NDVI), which employs information from the visible and near-infrared spectral regions (Los et al., 2005). Ideally, however, the physics underpinning the relationships between various environmental properties and satellite-sensor measurements of spectral reflectance should be represented explicitly, expressed analytically in mathematical terms (Verstraete et al., 1996). The resulting "physically-based" models can then be inverted against multispectral and multiangular measurements of surface reflectance to retrieve estimates of the models' driving parameters (i.e., the biophysical properties of the reflecting surface).

Several methods have been developed to optimize the inversion of physically-based models of surface reflectance with the aim of making them computationally efficient (Kimes et al., 2000). Approaches that employ Artificial Neural-Networks (ANNs) (Weiss et al., 2002) and look-up tables (LUTs) (North 2002b; Weiss & Baret 1999) are among the most widely used methods to solve the model inversion problem. For example, these approaches are used to derive a number of the global data products, including the LAI data sets produced from the MODIS and MISR sensors on board the Terra and Aqua satellites (Knyazikhin et al., 1998b). These LAI data sets are generated using a LUT approach, except under extreme conditions when the processing chain relies on a backup method based on a vegetation index. A similar approach is used to estimate LAI values from POLDER satellite-sensor data (Bicheron & Leroy 1999).

### 1.3. Integrated assessment of requirements

Here, we develop an end-to-end study, ranging from the collection of spectral reflectance data by the satellite-sensor to the estimation of various biophysical properties using LSP models. This approach enables us to analyse a number of satellite-sensor configurations and their likely impacts on the output from the LSP models. In particular, the relative value of multiangular and multispectral sensing capabilities, and the radiometric accuracy of the satellite-sensor, are analysed. The study focuses on the estimation of the following five surface biophysical properties: Fractional cover (FC), LAI, effective fraction of absorbed photosynthetically active radiation (fAPAR), leaf chlorophyll content and aerosol optical thickness (AOT), all of which can be estimated by means of satellite remote sensing (Grey et al., 2006; North, 2002b; Zarco-Tejada et al., 2004). AOT is included in this study to account for the effects of the atmosphere on the signal received by the satellite-sensor. The test site is a boreal forest, which represents an important biome in terms of the global carbon budget (Sellers et al., 1997b). Moreover, LSP models are typically sensitive to a range of surface properties for this biome type, enabling a robust evaluation of their uncertainty. This biome type is also structurally complex, providing a challenging test of the proposed method.

## 2. Method

This study examines the impact of various satellite-sensor properties on the estimation of NPP using each of two LSP models. A well-characterized scene is required, which is simulated by coupling three numerical models, namely: (i) a model of leaf spectral reflectance, PROSPECT (Jacquemoud & Baret 1990); a model of vegetation canopy reflectance, FLIGHT (North 1996; Pinty et al., 2006); and an atmospheric radiative-transfer model, Second Simulation of the Satellite Signal in the Solar Spectrum (6S) (Vermote et al., 1997). The scene simulations produced using these models are used to populate a LUT, which also serves to provide the spectral and angular reflectance samples employed in the biophysical property retrieval. The raw reflectance samples are also modulated by different levels of Gaussian noise, which is intended to represent radiometric noise in the sensor. The inversion of the coupled models using the LUT provides estimates of the surface biophysical properties for each spectral and angular sensor configuration. The value estimates in this way are subsequently used to drive the LSPs models and, hence, to estimate NPP (Fig. 1).

In order to make this study as representative a possible two LSP models were chosen as illustrative of medium and high complexity LSPs, namely BIOME-BGC 4.1.1 (White et al., 2000) and the Joint UK Land Environmental Simulator (JULES) (Alton et al., 2007; Essery et al., 2001). The test of the method in two different models will ensure that results are not artifacts produced by the internal parameterisations. BIOME-BGC is a multi-biome generalization of FOREST-BGC, a model originally developed to simulate the development of a forest stand through its life cycle. In BIOME-BGC, most ecosystem activity occurs at a daily time step (e.g., soil water balance, photosynthesis, allocation, litter fall, and C and N dynamics in the litter and soil), driven by daily values for precipitation, solar radiation, air humidity, and maximum and minimum air temperature. The surface is represented by single homogeneous vegetation canopy with a soil substrate. JULES is based on the UK Met Office Surface Exchange Scheme (MOSES). It uses a tiled land-surface scheme with 9 surface types (broad-leaf trees, needle-leaf trees, C3 grass, C4 grass, shrubs, urban, inland water, bare soil and ice). Each tile has different surface properties, including LAI, and the surface energy and water balances are aggregated across the tiles present in each gridbox. In JULES, the time step is defined by the meteorological data input to the model, and is typically 30 min. The inputs to both LSP models are climate, vegetation (including LAI), and site conditions data obtained from field campaigns.

### 2.1. Radiative-transfer simulation

The radiative-transfer simulation is performed in three steps, starting at the leaf level, progressing through to the canopy level, and ending at the top of the atmosphere (TOA) level (Fig. 1). The models involved in each of these stages are outlined briefly below.

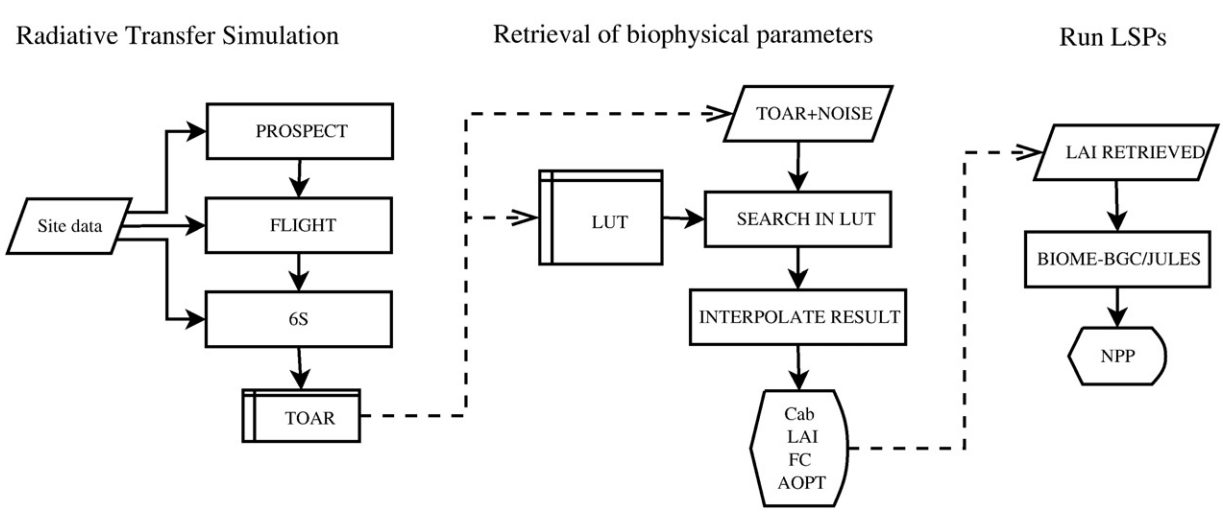


**Fig. 1.** Diagram of the methodology. TOA reflectance values are simulated by coupling a leaf reflectance model, a canopy reflectance model and an atmospheric radiative-transfer model. These TOA reflectance values are used to populate a LUT and to create the samples from which we want to retrieve the parameters. Biophysical parameters are retrieved from "noisy samples" by means of the LUT. LAI retrieved are used to drive the ecological models analysing the effects of the different levels of noise on the NPP estimated.

PROSPECT, a model of light interaction with leaves is used to estimate leaf reflectance and transmittance between 400 nm and 2500 nm. This model requires values of the following three parameters: a structure parameter (*N*), leaf chlorophyll content (Cab) and leaf water content (*W*).

A range of canopy reflectance models exist, from simple turbid-medium models to complex three-dimensional scene models. Scene simulation models produce realistic 3D scenes and photon interactions. Ray-tracing methods allow the sampling of photon trajectories and their intersections within the scene. The Monte Carlo method offers a robust and simple solution to this sampling scheme (Disney et al., 2000). In forward mode, rays are traced from the light source and followed through each of their interactions with the canopy until they reach the sensor position. This tends to be inefficient because a large number of photons are scattered in directions other than that of the sensor. In reverse mode, rays are traced from the sensor to the illumination hemisphere, which is more efficient in computational terms: this is the approach adopted here. The ray-tracing model used here, FLIGHT, requires data input on leaf, soil and bark optical properties and on canopy structure parameters. In reverse mode, FLIGHT simulates the spectral reflectance detected for a specific sun-sensor geometry (Alton et al., 2005; Barton & North, 2001).

The transmission of solar radiation through the atmosphere is affected by absorption and scattering caused by atmospheric molecules and aerosols. These effects must be considered when estimating the spectral and angular distribution of the downwelling solar radiation and in simulating the signal detected by a satellite-sensor. The 6S model computes gaseous absorption, Rayleigh scattering and optical scattering parameters for atmospheric aerosols. This model must be parameterized with specific data on atmospheric properties for the site of interest. In this study a clear atmosphere was considered based on the results measured during the field campaign (Walthall & Loechel, 1999). Subarctic summer atmospheric model and biomass aerosol model were used for the simulation. Using ground reflectance values as input, the model can provide an estimate of the TOA reflectance observed by a particular satellite-sensor.

### 2.2. Sensor models

Attention in this study is focused on a limited number of spectral wavebands. It is commonly reported that hyperspectral instruments typically contain considerable amounts of redundant spectral information, and that a subset of these bands can be used to obtain at least 90% of the total information content (Thenkabail et al., 2004). Therefore, we focus on a total of 14 spectral wavebands across the visible, near-infrared and short-wave infrared wavelengths.

The benefits of multiangular remote sensing are also analysed by simulating the observed spectral reflectance values under different viewing geometries (Barnsley et al., 1997; Diner et al., 1999). Two advantages are expected from this: first, it offers the potential to retrieve information on atmospheric constituents due to the effect of the different atmospheric path lengths on the TOA reflectance (Grey et al., 2006; North, 2002a,b; North et al., 1999); second, it should improve the retrieval of land-surface properties by accessing the structural information inherent in the Bidirectional Reflectance Distribution Function (BRDF) (Barnsley et al., 1997; Chen et al., 2003; Diner et al., 2005). In total, four instrument configurations are analysed, namely: (a) 1 view and 2 channels (1v/2b); (b) 1 view and 14 channels (1v/14b); (c) 9 views and 2 channels (9v/14b); and (d) 9 views and 14 channels (9v/14c). In the case of the 2 band evaluations, the selected channels lie in the red (630 nm) and near-infrared (870 nm) parts of the spectrum. In the case of the single viewing angle evaluation, each of the simulated angles is used to represent a wide-field-of-view cross-track instrument.

### 2.3. LUT inversion

As explained previously, the method chosen to invert the models is the LUT technique (Kimes et al., 2000). This approach is widely used across many disciplines and several studies have demonstrated the potential of using LUTs to solve the inversion problem in remote sensing, including in connection with the retrieval of vegetation canopy properties (Combal et al., 2002; Gascon et al., 2004; North 2002b; Weiss & Baret 1999). In remote sensing, the inverse problem is by nature ill-posed mainly for two reasons: first, the solution of the inverse problem is not necessarily unique, such that a set of solutions could lead to similar match between the measured and the simulated reflectance values; second, uncertainties in the measurements and the model may induce large variation in the solution of the inverse problem. To overcome this problem, we can constrain the model by making assumptions about some of the parameters (Combal et al., 2002). The constraints imposed here relate to the type of vegetation canopy, limited to coniferous forest, and the allowable range of values (i.e., maximum and minimum) for its biophysical properties limited to the range of values recorded in the field.

The LUT is implemented in three steps: (i) the parameter space of the canopy is sampled for a given sun-target-sensor geometry; (ii) for each combination of canopy parameters, TOA reflectance values are computed, which are used to populate the LUT (a set of test data is also generated that is used as the "observed" data in the retrieval); and (iii) the LUT is used to retrieve a set of estimated parameter values for the canopy by finding the best fit (minimum root mean square error (RMSE)) between the observed and simulated spectral profile.

#### 2.3.1. LUT sampling scheme

The density with which the data values in the LUT are sampled along each of the parameter axes affects the accuracy with which the biophysical properties are retrieved. Increasing the size of the LUT results in more accurate retrievals, but it also consumes greater computer resources (i.e., longer computation time). In general, therefore, the primary objective is to construct a LUT that is sufficiently sparse to allow quick access, but sufficiently dense to provide accurate retrievals. The key is to obtain a compromise between these two competing requirements.

A view zenith angle configuration corresponding to that of the MISR instrument is analysed here (Table 2). This is intended to explore the advantages of the sensor having the capability to acquire data at several different view angles. The analysis is performed for data acquired in the solar principal plane only, which is normally the direction of the maximum angular variability in the detected spectral reflectance. In reality, the relative azimuth angle of most satellite-sensor measurements will deviate from this plane, and depends on the relative positions of the satellite and the sun. Although these are not very realistic scenarios, they allow us to examine the effect of multiangular sensing in the most extreme case of backward and forward scattering. The range of spectral wavebands used here correspond to those employed by a range of current satellite-sensors (Table 2; AVHRR, MODIS, MISR, MERIS, VEGETATION and CHRIS), which have proved to be useful in the retrieval of surface biophysical properties (Abuelgasim et al., 2006; Barnsley et al., 2000; Knyazikhin et al., 1998b).

The range of values over which the biophysical properties are sampled in the LUT is derived from the values typically observed in field data. The sample points are positioned to maximize the variability in the parameter space captured by the LUT. For some biophysical properties, such as LAI, a regular sampling strategy may result in under-sampling at the lower end of the expected LAI range,

**Table 2**
Viewing and spectral capabilities simulated

| Parameter | Values | Comments |
|---|---|---|
| View zenith angles | ±70.5°, ±60°, ±45.6°, ±26.1°, 0° | MISR viewing zenith angles |
| Channels | 440, 460, 490, 550, 620, 670, 700, 800, 840, 860, 870, 900, 1240 and 1600 nm | |

**Table 3**
Transformations applied to sample the input parameters

| Variable transformation | |
|---|---|
| LAI | $\exp^{-LAI/2}$ |
| $C_{ab}$ | $\exp^{-Cab/100}$ |
| FC | FC |

where the detected reflectance normally varies significantly. To guarantee uniform sampling, therefore, the biophysical properties are re-sampled on a transformed space, which is created taking into account the expected distribution of each property. Thus, the distribution function of each property is analysed to define the optimal sampling scheme. In this context, we note that fractional cover exhibits a broadly linear relationship with reflectance, while transformations similar to those used in other studies (Combal et al., 2002; Weiss & Baret, 1999) are applied to LAI and Cab (Table 3).

The optimal number of samples, which defines the size and density of the LUT, was evaluated in a pilot study, using 3, 6 or 12 samples for each of the biophysical properties examined here (FC, Cab and LAI). For AOT, only two values are used: a maximum value (0.15) and a minimum value (0.05).

The results of the pilot study, not presented here, indicate that 6 samples is optimal for each of the biophysical properties except for LAI, for which 12 samples must be used at sites that exhibit a large range of LAI values. While LAI, Cab and FC are included in the LUT from the outset based on the specified input values, fAPAR is estimated separately using FLIGHT and is included in the LUT at a later stage. fAPAR is calculated as the sum of the absorbed radiation at each wavelength as follows:

$$\mathrm{fAPAR} = \sum_{i=1}^{n} F_{a,i} W_i \tag{1}$$

where $F_{a,i}$ is the fraction of radiant energy absorbed by the canopy in waveband $i$, calculated using FLIGHT, and $W_i$ are the weights given to each waveband according to the solar irradiance in that waveband determined from 6S (Privette et al., 1996). Only bands in the photosynthetically active radiation range are used (i.e., 400 nm to 700 nm).

For each combination of input parameter values, the TOA reflectance is calculated and is stored with the corresponding input parameter values in the LUT. These values create the LUT that is used in the inversion procedure to retrieve estimates of the same parameters.

### 2.3.2. Sensor noise

The effect of the radiometric accuracy of the sensor on the measurement of surface-leaving radiances is simulated through the addition of different levels of noise. In remote sensing, noise is produced by a number of factors, including thermal effects, sensor saturation, quantization errors and transmission errors. These types of noise are typically independent of the data, and are generally additive in nature so that they can be represented reasonably well by a normally distributed (i.e., Gaussian) random process with a mean value of zero and a probability density function given as follows:

$$f(x) = \frac{1}{\sigma_n \sqrt{2\pi}} e^{-x^2/2\sigma_n^2} \tag{2}$$

where $\sigma_n$ is the standard deviation of the noise process(es).

In this study, the effect of noise is modelled as the summation of the true signal and the noise. Gaussian noise, ranging from 0.0 to 0.05, in steps of 0.005, is added to the reflectance values of the test data. The resultant noisy reflectance values are then used to retrieve estimates of the biophysical properties from the LUT.

### 2.3.3. LUT parameters retrieval

Estimates of the vegetation canopy properties are obtained by minimising the difference between the reflectance values in the simulated input data and those in the LUT. This problem is solved here, as in many other studies, using the standard least-squares approach (Knyazikhin et al., 1998a; Weiss et al., 2000).

To establish the most likely values of the surface biophysical properties, the set of errors produced by comparing the observed and simulated reflectance spectra is filtered to identify one or more candidate solutions. In circumstances where there is more than one candidate solution, the optimum solution is typically determined by calculating the median or the weighted mean of the parameter values for the candidate solutions (Weiss & Baret, 1999). Here, we apply a gridded sampling in the creation of the LUT and a random sampling for the "observed" data. The final result is interpolated between the retrieved best candidates.

The algorithm used here compares the observed reflectance values to the simulated reflectance values stored in the LUT; the RMSE is used to retrieve a set of possible (or candidate) solutions. A maximum of 10 candidate solutions is allowed, consisting of those producing the minimum RMSE values. The absolute RMSE is calculated as follows:

$$\mathrm{RMSE} = \sqrt{\frac{1}{n}\sum_{i=1}^{n}\left(\rho_{\mathrm{LUT},i} - \rho_{\mathrm{Input},i}\right)^2} \tag{3}$$

where $n$ is the number of spectral wavebands multiplied by the number of sensor view angles considered. The absolute RMSE is used rather than the relative RMSE because the Gaussian noise is additive and using relative errors would mask the effect of the noise.

The optimum result should lie somewhere in the neighbourhood of the candidate set of solutions. The final result is therefore taken to be an interpolation of the best candidate solutions. The method used to do this is to select only those candidates for which the RMSE is smaller than a threshold value, calculated as a function of the minimum RMSE, i.e., if $\mathrm{RMSE}_i \leq \mathrm{MinRMSE} + (\alpha \times \mathrm{MinRMSE})$, where $\alpha$

**Table 4**
Sites and stands data

| | OBS | OJP | YJP | Source |
|---|---|---|---|---|
| Dominant species | Black spruce (*Picea mariana*) | Jack pine (*Pinus banksiana*) | Jack pine (*Pinus banksiana*) | |
| Latitude | 53.987°N | 53.916°N | 53.877°N | |
| Longitude | 105.122°W | 104.692°W | 104.647°W | |
| Age years | 115 | 65 | 25 | Gower et al. (1997) |
| e/c | C | C | C | |
| Exy (m) | 0.45 | 1.3 | 0.85 | Leblanc et al. (1999) |
| Ez (m) | 9 | 7.2 | 4 | Leblanc et al. (1999) |
| Min_HT (m) | 0.49 | 6.9 | 0.49 | Leblanc et al. (1999) |
| Max_HT (m) | 0.51 | 7.1 | 0.51 | Leblanc et al. (1999) |
| DBH (m) | 0.071 | 0.129 | 0.032 | Gower et al. (1997) |
| Leaf size (m) | 0.01 | 0.01 | 0.01 | Estimation |

e/c: shape (ellipsoid or cone); Exy: crown radius; Ez: crown height; Min_HT, Max_HT: minimum and maximum height to first branch; DBH: diameter at breast height.

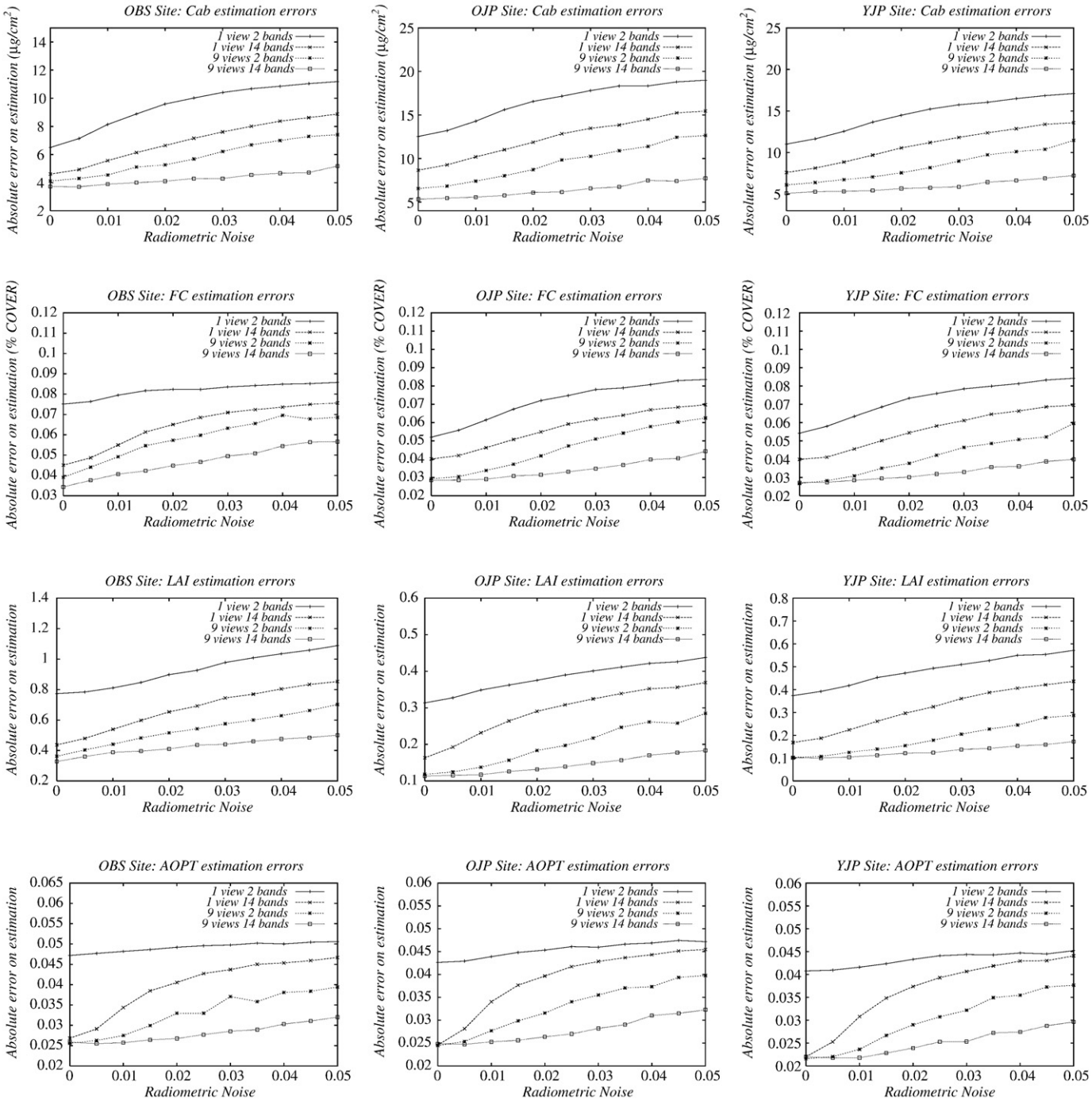


**Fig. 2.** Parameter estimations represented against the level of radiometric noise for the three sites (OBS, OJP and YJP) and for each configuration.

represents the percentage of deviation from the MinRMSE accepted. The value of $\alpha$ varies with the instrument radiometric noise, Noise, considered in each case, with a minimum value of 10%:

$$\alpha = 0.1 + \text{Noise}. \tag{4}$$

The final result for each estimated parameter is calculated as a weighted average of the set of candidate solutions. The weights applied to each of the retrieved parameters are calculated as follows:

$$W_i = \left(1 - \frac{RMSE_i}{\sum RMSE}\right) / (n-1) \tag{5}$$

where $n$ is the number of candidate solutions used in the interpolation, and $i$ varies from 1 to $n$.

With this technique, we ensure that at least one value will be retrieved, the one with the minimum RMSE. Also, this approach allows us to consider up to 10 possible candidate solutions, among which to interpolate, discarding those solutions for which the RMSE is too large.

### 2.3.4. Coupling with LSPs

The effective LAI values used in the creation of the LUT are also employed as inputs to the LSP models. The current generation of LSPs models cannot use the other parameters, such as Cab, directly; however, joint retrieval of Cab and LAI tends to reduce uncertainty in

**Table 5**
Effect of solar zenith angle on the retrieval of parameters

| | RMSE | 40° | 50° | 60° | 70° |
|---|---|---|---|---|---|
| $C_{ab}$ | $E_{abs}$ | 3.57 | 4.22 | 5.00 | 6.95 |
| | $E_{rel}$ | 0.12 | 0.15 | 0.18 | 0.27 |
| FC | $E_{abs}$ | 0.02 | 0.026 | 0.034 | 0.051 |
| | $E_{rel}$ | 0.05 | 0.07 | 0.09 | 0.15 |
| LAI | $E_{abs}$ | 0.15 | 0.18 | 0.20 | 0.27 |
| | $E_{rel}$ | 0.07 | 0.08 | 0.09 | 0.13 |
| fAPAR | $E_{abs}$ | 0.015 | 0.016 | 0.018 | 0.025 |
| | $E_{rel}$ | 0.03 | 0.04 | 0.04 | 0.05 |
| AOPT | $E_{abs}$ | 0.02 | 0.023 | 0.026 | 0.028 |
| | $E_{rel}$ | 0.21 | 0.24 | 0.27 | 0.29 |

Absolute and relative RMSE of the retrieved parameters are shown for each solar zenith angle for the case of 9 viewing angles and 14 bands and a noise of 0.01 absolute value. Errors are calculated as mean values of the three sites.

the estimated values of LAI (Dawson et al., 1999, 2003). Moreover, in their current form, both of the LSP models considered here are insensitive to variability in the ratio of direct to diffuse sunlight associated with the different values of atmospheric optical depth examined in this study (Alton et al., 2005).

In JULES, LAI is an input parameter so no modifications are required to this model. BIOME-BGC, by contrast, predicts the projected LAI as a function of the amount of leaf carbon and the canopy-average specific leaf area. BIOME-BGC was therefore modified in this study, such that it was forced to use the effective LAI specified on input rather than relying on the value produced by its own internal calculations, corresponding to driving the model with the observed LAI.

Note that both LSP models studied here are "spun up" by running them for a repeating pattern of annual weather conditions, corresponding to a period of two years. The time step used was 30 min in both models and the meteorological data were taken from the field measurements. The value of annual NPP output for the second year is then recorded.

### 2.4. Site description

A boreal forest biome is used as test site in this study because of the significance of this biome type in terms of regional and global carbon budgets. Moreover, the structural complexity of this biome type provides a good test of the methodology adopted here. The LSP models studied in this paper are also sensitive to the range of vegetation parameters exhibited by boreal forest biomes, enabling a robust test of their uncertainty.

Boreal forests encircle Earth at latitudes above 48°N and comprise roughly 21% of the global forest area. The main influence of boreal forests on the climate system is through its potential to sequester and release large volumes of carbon. In the long term, expected trends in atmospheric warming may lead to dramatic changes in the global carbon cycle, by affecting the ability of boreal forest ecosystems to sequester carbon through enhanced photosynthesis and release carbon through increased respiration (Baldocchi et al., 2000; Bonan et al., 1995). Over shorter time scales, boreal forests play a significant role in seasonal and annual climates by masking the high albedo of snow on the ground and through the partitioning of net radiation into sensible and latent heat.

The Boreal Ecosystem Atmospheric Study (BOREAS) was an international project, which ran between 1993 and 1996, focusing on the northern boreal forests of Canada with the aim of better understanding the interactions between such forests and the atmosphere (Gamon et al., 2004; Sellers et al., 1997b). Here, we concentrate on the Southern Study Area (SSA), analysing data collected during the 1994 field campaign. The SSA is situated near Candle Lake, Saskatchewan, and covers an area about 130 km by 90 km. The vegetation cover is predominantly coniferous forest, typically classified as mixed boreal forest. The SSA experiences a mid-continental climate with average annual precipitation ranging from 410 mm to 500 mm. Temperatures range from about 7 °C to 24 °C in the summer and from about −21 °C to −4 °C in the winter.

Three sub-sites are explored here, each with a different dominant tree species, namely: (i) old black spruce (OBS), (ii) young jack pine (YJP) and (iii) old jack pine (OJP) (Table 4).

### 2.5. Test data

Solar zenith angles were sampled in the range 40° to 70°, at intervals of 10°, corresponding to the sun angles experienced at high latitudes. An independent set of 200 TOAs reflectance spectra, representing the "observed" data, was created using the methods outlined in the previous sections. These values are subsequently used as the inputs to the inversion procedure. The reflectance spectra were simulated based on randomly sampled values of the biophysical properties within the specified ranges. Each of these TOAs reflectance data sets comprises values in 14 spectral channels and 9 sensor view angles corresponding with MISR viewing angles (Table 2). These data sets are used for the retrieval of surface properties in each of the four angular/spectral configurations described previously, by selecting the appropriate subset of view zenith angles and spectral wavebands.

The effective LAI values estimated in the inversion procedure are used to drive the two LSP models. Effective LAI is used instead of LAI corrected for clumping effects (Chen et al., 1997) in both models. BIOME-BGC uses projected LAI in its internal calculations, which is assumed to be equivalent to the effective LAI here. JULES uses radiation interception to estimate productivity: as there is no consideration of clumping in this calculation, effective LAI is considered to be the more appropriate value.

The LSP models are parameterised using the data collected in the BOREAS field campaign (Cuenca et al., 1997; Kimball et al., 1997b). Both models show a high degree of sensitivity to soil properties, especially the soil moisture content. A "spin up" period is required to settle the models in terms of these parameters, so that they produce stable results.

## 3. Results for a boreal forest biome

### 3.1. Biophysical property retrieval

The accuracy with which the surface biophysical property values are retrieved is analysed in terms of the absolute mean error (RMSE) between the observed (input) and retrieved values. Fig. 2 shows the results for each of the properties measured against different levels of sensor. This figure indicates that there is a difference between the observed and retrieved values even in the presence of zero sensor noise. This is due partly to the different combinations of input biophysical property values that produce quite similar reflectance spectra, leading to the identification of several candidate solutions by the inversion procedure and, hence, to the observed errors; and partly to the sampling density of the LUT. There is also an intrinsic error introduced by the Monte Carlo simulation. Since Monte Carlo methods are stochastic, simulations contain statistical fluctuations inversely proportional to the square root of the number of photon trajectories considered. In this study, these fluctuations are in the range of ±0.002 absolute error.

The effect of sensor noise can be summarised as follows: the retrievals show a smooth, near linear, increase in error with increasing sensor noise.

In general, it is also clear that the retrieval of surface biophysical properties is improved in all cases where multiple view angle data are employed. The minimum instrument configuration, namely a single sensor view angle and just 2 spectral wavebands, leads to the greatest errors in all cases, but is especially incapable of detecting accurately the AOT, which indirectly affects the estimation of the other property values.

Retrievals of Cab and FC made using data recorded at a single sensor view angle in 14 spectral wavebands are similar in accuracy to those obtained with multiple view angle data recorded and the lowest

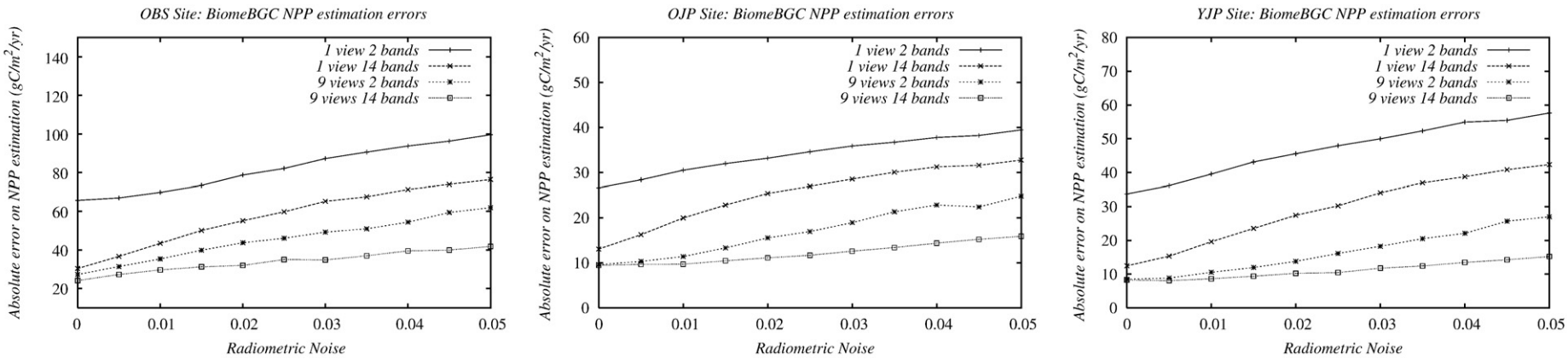


**Fig. 3.** Effect of the instrument radiometric noise on the NPP estimated by Biome-BGC at each site and for each instrument configuration.

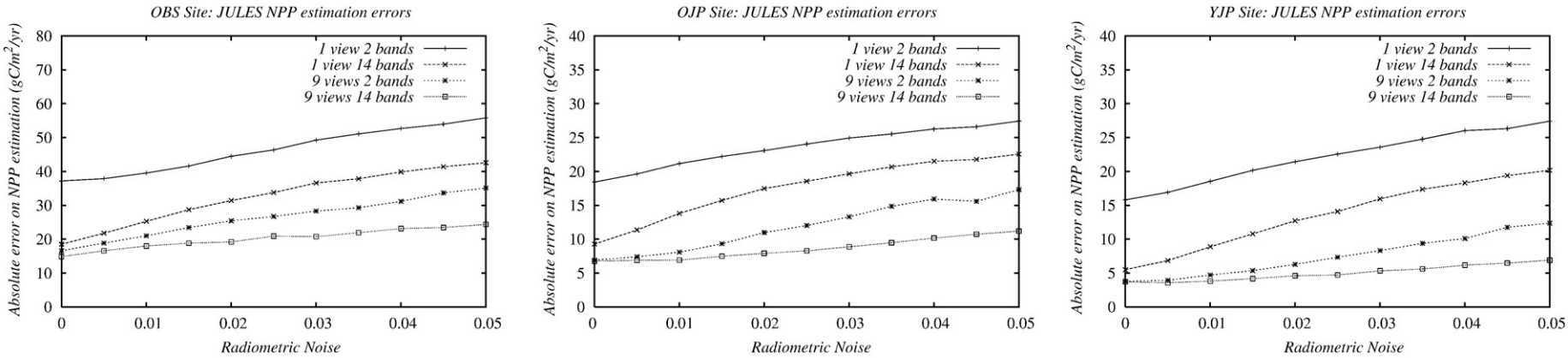


**Fig. 4.** Effect of the instrument radiometric noise on the NPP estimated by JULES at each site and for each instrument configuration.

levels of sensor noise (0.005), but the error increases rapidly at higher levels of noise.

Retrievals obtained using data recorded at 9 sensor view angles provide roughly double the accuracy (i.e., half the error) of the respective configurations (i.e., 2 and 14 bands) made at a single sensor view angle. In these cases, sensor noise has a relatively small effect, especially in terms of the retrieval of LAI, showing the significance of multiple view angle data for the retrieval of information of vegetation canopy structure.

In analysing the effect of atmospheric properties on the retrievals, each solar zenith angle is shown separately in Table 5. Not surprisingly, the best retrievals are obtained when the solar zenith angle is small because the effect of the atmosphere is reduced due to the atmospheric shorter path-length.

### 3.2. LSP sensitivity

The annual NPP estimated by each model is recorded. Errors are analysed in terms of the mean absolute difference between the NPP values obtained with the actual LAI (i.e., the field measurements) and the LAI estimated by inversion of the LUTs against the simulated satellite-sensor data. This process is repeated for each site and for the four hypothetical instrument configurations. The results are also presented in terms of the different levels of simulated sensor noise (Figs. 3 and 4). In summary, the trends are similar to those observed in the figures for the biophysical properties reported in the previous section, with the multiple view angle data producing the most accurate results, even in the presence of just two spectral bands.

The values of NPP estimated by the two LSP models, for an estimated average effective LAI of 2.3 (OBS), 1.7 (OJP) and 1.5 (YJP) (Chen et al., 1997) are 209 gC $m^{-2}$ $yr^{-1}$ (OBS), 181 gC $m^{-2}$ $yr^{-1}$ (OJP) and 135 gC $m^{-2}$ $yr^{-1}$ (YJP) for Biome-BGC and 203 gC $m^{-2}$ $yr^{-1}$ (OBS), 180 gC $m^{-2}$ $yr^{-1}$ (OJP) and 178 gC $m^{-2}$ $yr^{-1}$ (YJP) for JULES. These values fall in the range of values reported from field measurements (Gower et al., 1997) and simulations (Kimball et al., 1997a) for the same sites.

As in the case of the retrieval of surface biophysical properties, the configuration with 9 sensor view angles and 14 spectral wavebands performed best, regardless of the level of sensor noise, and no magnification of the errors was detected. The next best results were obtained using data recorded at 9 sensor view angles in two spectral bands. In the 1v/14b configuration and a radiometric noise level of 0.01, the errors on the estimated NPP range between 19.6 gC $m^{-2}$ $yr^{-1}$ (YJP, Biome-BGC) and 43.5 gC $m^{-2}$ $yr^{-1}$ (OBS, Biome-BGC). The 9v/14b configuration produces a 31% to 56% improvement on these figures, with errors ranging from 8.6 gC $m^{-2}$ $yr^{-1}$ (YJP, Biome-BGC) to 29. gC $m^{-2}$ $yr^{-1}$ (OBS, Biome-BGC). Doubling the radiometric accuracy from 0.02 to 0.01 produces improvements of around 10%, 25%, 20% and 15%, respectively, for each of the following sensor configurations: 1v/2b, 1v/14b, 9v/2b and 9v/14b. Increasing the number of spectral wavebands from 2 to 14 produces improvements of between 30% and 50% at noise levels under 0.015 for data recorded at a single view angle. Where the same data are recorded at 9 different view angles, the improvement obtained by the higher spectral sampling is smaller: only 10% to 20%.

In general, we find that JULES is less sensitive to the effective LAI inputs, and hence to errors on these, than Biome-BGC. As an example, for a level of noise of 0.01 and the most comprehensive sensor configuration (9v/14b), NPP errors derived from JULES are 18.0 gC $m^{-2}$ $yr^{-1}$ (OBS), 6.9 gC $m^{-2}$ $yr^{-1}$ (OJP) and 3.8 gC $m^{-2}$ $yr^{-1}$ (YJP), while the corresponding values for Biome-BGC are 29.7 gC $m^{-2}$ $yr^{-1}$, 9.7 gC $m^{-2}$ $yr^{-1}$ and 7.8 gC $m^{-2}$ $yr^{-1}$.

Overall, the results show a clear advantage of the multiangular sampling over the other sensor configurations analysed. Note that these results relate to coniferous forest sites, and it is possible that they are specific to such sites. Boreal forests have a complex three-dimensional structure, for which a multiple view angle capability is likely to be important. Single angle observations (e.g., at nadir) are not able to capture the structure of the forest canopy, so that measurements such as these may produce less accurate estimates of surface biophysical properties and NPP.

## 4. Conclusions

A method is presented here that links satellite instrument capabilities with LSP models. The results of this method suggest that satellite-sensor data recorded at multiple view angles improves dramatically the accuracy with which surface biophysical properties can be estimated, even in the presence of a limited number of spectral wavebands. Satellite-sensor data obtained at multiple view angles provide structural information critical to characterize the type of coniferous forests analysed here. A more comprehensive spectral sampling (i.e., increasing the number of spectral channels from 2 to 14) also reduces the error with which the surface properties are estimated (by over 50% for data recorded at a single view angle), although the impact of this is smaller in the case of multiple view angle data (10% to 20%). The radiometric accuracy of the sensor, simulated through different levels of additive noise, does not appear to produce such a large relative effect on the accuracy of the biophysical property retrievals, with only a 10% to 25% improvement obtained by halving the radiometric noise from 0.02 to 0.01.

The conclusion that we draw from this analysis, therefore, is that the inclusion of multiple view angle capabilities in future satellite-sensors targeted at monitoring Earth's surface is likely to improve significantly the retrieval of information on surface biophysical properties and, in particular, the intrinsic structural characteristics of vegetation canopies. Spectral information and radiometric accuracy are less critical if a multiple view angle capability is available, but the relative cost of each must also be considered when designing instruments.

## Acknowledgements

This study has been funded by the National Physical Laboratory (NPL) and supported by NERC Climate and Land-Surface Systems Interaction Centre (CLASSIC). Biome-BGC version 4.1.1 was provided by the Numerical Terradynamic Simulation Group (NTSG) at the University of Montana.

## References

Abuelgasim, A., Fernandes, R., & Leblanc, S. (2006). Evaluation of national and global LAI products derived from optical remote sensing instruments over Canada. *IEEE Transactions on Geoscience and Remote Sensing*, *44*, 1872–1884.

Alton, P., Mercado, L., & North, P. (2007). A sensitivity analysis of the land-surface scheme JULES conducted for three forest biomes: Biophysical parameters, model processes, and meteorological driving data. *Global Biogeochemical Cycles*, *20*, GB1008. doi:10.1029/2005GB002653

Alton, P., North, P., Kaduk, J., & Los, S. (2005). Radiative transfer modelling of direct and diffuse sunlight in a Siberian pine forest. *Journal of Geophysical Research*, *110*, D23209.

Baldocchi, D., Kelliher, F., Black, T., & Jarvis, P. (2000). Climate and vegetation controls on boreal zone energy exchange. *Global Change Biology*, *6*, 69–83.

Barnsley, M., Lewis, P., O'Dwyer, S., Disney, M., Hobson, P., Cutter, M., et al. (2000). On the potential of CHRIS-PROBA for estimating vegetation canopy properties from space. *Remote Sensing Reviews*, *19*, 171–189.

Barnsley, M. J., Allison, D., & Lewis, P. (1997). On the information content of multiple view angle (MVA) images. *International Journal of Remote Sensing*, *18*, 1937–1960.

Barton, C., & North, P. (2001). Remote sensing of canopy light use efficiency using the photochemical reflectance index: Model and sensitivity analysis. *Remote Sensing of Environment*, *78*, 164–273.

Bicheron, P., & Leroy, M. (1999). A Method of biophysical parameter retrieval at global scale by inversion of a vegetation reflectance model. *Remote Sensing of Environment*, 251–266.

Bonan, G., Chapin, F., & Thompson, S. (1995). Boreal forest and tundra ecosystems as components of the climate system. *Climatic Change*, *29*, 145–167.

Canadell, J., Dickson, R., Hibbard, K., Raupach, M., & Young, O. (2003). Science framework and implementation. *Global Carbon Project Report No. 1 1, Global Carbon Project*.

Chen, J., Liu, J., Leblanc, S., Lacaze, R., & Roujean, J. (2003). Multi-angular optical remote sensing for assessing vegetation structure and carbon absorption. *Remote Sensing of Environment*, *84*, 516–525.

Chen, J. M., Rich, P. M., Gower, S. T., Norman, J. M., & Plummer, S. (1997). Leaf area index of boreal forests: Theory, techniques, and measurements. *Journal of Geophysical Research*, 29429–29443.

Combal, B., Baret, F., Weiss, M., Trubuil, A., Mace, D., Pragnere, A., et al. (2002). Retrieval of canopy biophysical variables from bidirectional reflectance. Using prior information to solve the ill-posed inverse problem. *Remote Sensing of Environment*, *84*, 1–15.

Cox, P., Betts, R., Bunton, C. B., Essery, R., Rowntree, P., & Smith, J. (1999). The impact of new land surface physics on the GCM simulation of climate and climate sensitivity. *Climate Dynamics*, 183–203.

Cramer, W., Bondeau, A., Woodward, F. I., Prentice, I. C., Betts, R. A., Brovkin, V., et al. (2001). Global response of terrestrial ecosystem structure and function to CO2 and climate change: Results from six dynamic global vegetation models. *Global Change Biology*, 357–373.

Cuenca, R., Stangel, D., & Kelly, S. (1997). Soil water balance in a boreal forest. *Journal of Geophysical Research-Atmospheres*, *102*, 29355–29365.

Dawson, T., Curran, P., North, P., & Plummer, S. (1999). The propagation of foliar biochemical absorption features in forest canopy reflectance. *Remote Sensing of Environment*, *67*, 147–159.

Dawson, T., North, P., Plummer, S. E., & Curran, P. (2003). Forest ecosystem chlorophyll content: Implications for remotely sensed estimates of net primary productivity. *International Journal of Remote Sensing*, *24*, 611–617.

Diner, D., Braswell, B., Davies, R., Gobron, N., Hu, J., Jin, Y., et al. (2005). The value of multiangle measurements for retrieving structurally and radiatively consistent properties of clouds, aerosols, and surfaces. *Remote Sensing of Environment*, *97*, 495–518.

Diner, D. J., Asner, G. P., Davies, R., Knyazikhin, Y., Muller, J. P., Nolin, A. W., et al. (1999). New directions in Earth observing: Scientific application of multi-angle remote sensing. *Bulletin of the American Meteorological Society*, *80*, 2209–2228.

Disney, M. I., Lewis, P., & North, P. (2000). Monte Carlo methods in optical canopy reflectance modelling. *Remote Sensing Reviews*, *18*, 163–196.

Essery, R., Best, M., & Cox, P. (2001). *MOSES 2.2 Technical Documentation., Technical note, 30., Hadley Centre, Bracknell, UK*.

Friedl, M., McIver, D., Hodges, J., Zhang, X., Muchoney, D., Strahler, A., et al. (2002). Global land cover mapping from MODIS: Algorithms and early results. *Remote Sensing of Environment*, *83*, 287–302.

Gamon, J., Huemmrich, K., Peddle, D., Chen, J., Fuentes, D., Hall, F., et al. (2004). Remote sensing in Boreas: Lessons learned. *Remote Sensing of Environment*, *89*, 139–162.

Gascon, F., Gastellu-Etchegorry, J. P., Lefevre-Fonollosa, M. -J., & Dufrene, E. (2004). Retrieval of forest biophysical variables by inverting a 3-D radiative transfer model and using high and very high resolution imagery. *International Journal of Remote Sensing*, *25*, 5601–5616.

Gower, S., Vogel, J., Norman, J., Kucharik, C., Steele, S., & Stow, T. (1997). Carbon distribution and aboveground net primary production in aspen, jack pine, and black spruce stands in Saskatchewan and Manitoba, Canada. *Journal of Geophysical Research-Atmospheres*, *102*, 29029–29041.

Grey, W., North, P., Los, S., & Mitchell, R. (2006). Aerosol optical depth and land surface reflectance from multi-angle AATSR measurements: Global validation and inter-sensor comparisons. *IEEE Transactions on Geoscience and Remote Sensing*, *44*, 2184–2197.

Heinsch, F., Zhao, M., Running, S., Kimball, J., Nemani, R., Davis, K., et al. (2006). Evaluation of remote sensing based terrestrial productivity from MODIS using regional tower eddy flux network observations. *IEEE Transactions on Geoscience and Remote Sensing*, *44*, 1908–1925.

IPCC (2001). *Climate change 2001: The scientific basis.* : Cambridge University Press.

IPCC (2007). *Climate change 2007: The physical science basis.* : Cambridge University Press.

Jacquemoud, S., & Baret, F. (1990). PROSPECT: A model of leaf optical properties spectra. *Remote Sensing of Environment*, *34*, 75–91.

Kimball, J., Thornton, P., White, M., & Running, S. (1997). Simulating forest productivity and surface–atmosphere carbon exchange in the BOREAS study region. *Tree Physiology*, *17*, 589–599.

Kimball, J., White, M., & Running, S. (1997). BIOME-BGC simulations of BOREAS stand hydrologic processes. *Journal of Geophysical Research*, *102*, 29.043–29.051.

Kimes, D., Knyazikhin, Y., Privette, J., Abuelgasim, A., & Gao, F. (2000). Inversion methods for physically-based models. *Remote Sensing Reviews*, *18*, 381–439.

Knyazikhin, Y., Martonchik, J. V., Diner, D. J., Myneni, R. B., Verstraete, M. M., Pinty, B., et al. (1998). Estimation of vegetation canopy leaf area index and fraction of absorbed photosynthetically active radiation from atmosphere corrected MISR data. *Journal of Geophysics*, *103*, 32239–32256.

Knyazikhin, Y., Martonchik, J. V., Myneni, R. B., Diner, D. J., & Running, S. (1998). Synergistic algorithm for estimating vegetation canopy leaf area index and fraction of absorbed photosynthetically active radiation from MODIS and MISR data. *Journal of Geophysical Research*, *103*, 32257–32276.

Lambin, E., & Linderman, M. (2006). Time series of remote sensing data for land change science. *IEEE Transactions on Geoscience and Remote Sensing*, *44*, 1926–1928.

Leblanc, S., Bicheron, P., Chen, J., Leroy, M., & Cihlar, J. (1999). Investigation of directional reflectance in boreal forests with an improved four-scale model and airborne POLDER data. *IEEE Transactions on Geoscience and Remote Sensing*, *37*, 1396–1414.

Los, S., North, P., Grey, W., & Barnsley, M. (2005). A method to convert AVHRR Normalised Difference Vegetation Index time-series to a standard viewing and illumination geometry. *Remote Sensing of Environment*, *99*, 400–411.

Morisette, J., Privette, J., & Justice, C. (2002). A framework for the validation of MODIS Land products. *Remote Sensing of Environment*, *83*, 77–96.

North, P. (1996). Three-dimensional forest light interaction model using a Monte Carlo method. *IEEE Transactions on Geoscience and Remote Sensing*, *34*, 946–956.

North, P. (2002). Estimation of aerosol opacity and land surface bidirectional reflectance from ATSR-2 dual-angle imagery: Operational method and validation.*Journal of Geophysical Research*, *107* No. 4149.

North, P. (2002). Estimation of fAPAR, LAI and vegetation fractional cover from ATSR-2 imagery. *Remote Sensing of Environment*, *80*, 114–121.

North, P. R. J., Briggs, S., Plummer, S., & Settle, J. (1999). Retrieval of land surface bdirectional reflectance and aerosol opacity from ATSR-2 multiangle imagery. *IEEE Transactions on Geoscience and Remote Sensing*, *37*, 526–537.

Pinty, B., Widlowski, J. -L., Taberner, M., Gobron, N., Verstraete, M. M., Disney, M., et al. (2006). Radiation Transfer Model Intercomparison (RAMI) exercise: Results from the second phase. *Journal of Geophysical Research*, *109*.

Plummer, S. E. (2000). Perspectives on combining ecological process models and remotely sensed data. *Ecological Modelling*, *129*, 169–186.

Potter, C., Klooster, S., Steinbach, M., Tan, P., Kumar, V., Shekhar, S., et al. (2003). Global teleconnections of climate to terrestrial carbon flux. *Journal of Geophysical Research*, *108*, 4556.

Privette, J., Myneni, R., Emery, W., & Hall, F. (1996). Optimal sampling conditions for estimating grassland parameters via reflectance model inversions. *IEEE Transactions on Geoscience and Remote Sensing*, *34*, 272–284.

Raupach, M., Rayner, P., Barrett, D., Defries, R., Heimann, M., Ojima, D., et al. (2005). Model-data synthesis in terrestrial carbon observation: Methods, data requirements and data uncertainty specifications. *Global Change Biology*, *11*, 378–397.

Sellers, P., Dickinson, R., Randall, D., Betts, A., Hall, F., Berry, J., et al. (1997). Modeling the exchanges of energy, water, and carbon between continents and the atmosphere. *Science*, *275*, 502–509.

Sellers, P., Hall, F., Kelly, R., Black, A., Baldocchi, D., Berry, J., et al. (1997). BOREAS in 1997: Experiment overview, scientific results and future directions. *Journal of Geophysical Research*, *102*, 28,731–28,770.

Sellers, P., Meeson, B., Hall, F., Asrar, G., Murphy, R., Schiffer, R., et al. (1995). Remote sensing of the land surface for studies of global change: Models–algorithms–experiments. *Remote Sensing of Environment*, *51*, 3–26.

Thenkabail, P., Enclona, E., Ashton, M., & Van Der Meer, V. (2004). Accuracy assessments of hyperspectral waveband performance for vegetation analysis applications. *Remote Sensing of Environment*, *91*, 354–376.

Townshend, J., & Justice, C. (2002). Towards operational monitoring of terrestrial systems by moderate-resolution remote sensing. *Remote Sensing of Environment*, *83*, 351–359.

Turner, D., Ritts, W., Cohen, W., Gower, S., Running, S., Zhao, M., et al. (2006). Evaluation of MODIS NPP and GPP products across multiple biomes. *Remote Sensing of Environment*, *102*, 282–292.

Turner, D., S.V., O., & Kimball, J. (2004). Integrating remote sensing and ecosystem process models for landscape to regional scale analysis of the carbon cycle. *Bioscience*, *54*, 573–584.

Vermote, E., Tanre, D., Deuze, J., Herman, M., & Morcrette, J. (1997). Second simulation of the satellite signal in the solar spectrum: An overview. *IEEE Transactions on Geoscience and Remote Sensing*, *35*, 675–686.

Verstraete, M., Pinty, B., & Myneni, R. (1996). Potential and limitations of information extraction on the terrestrial biosphere from satellite remote sensing. *Remote Sensing of the Environment*, *58*, 201–214.

Walthall, C. L., & Loechel, S. (1999). *BOREAS RSS-03 atmospheric conditions from a helicopter-mounted sunphotometer.* Data set., Available on-line [http://www.daac.ornl.gov] from Oak Ridge National Laboratory Distributed Active Archive Center, Oak Ridge, Tennessee, U.S.A.

Weiss, M., & Baret, F. (1999). Investigation of a model inversion technique to estimate canopy biophysical variables from spectral and directional reflectance data. *Remote Sensing of Environment*, *70*, 293–306.

Weiss, M., Baret, F., Leroy, M., Hautecoeur, O., Bacour, C., Prevot, L., et al. (2002). Validation of neural net techniques to estimate canopy biophysical variables from remote sensing data. *Agronomie*, *22*, 547–553.

Weiss, M., Baret, F., Myneni, R., Pragnere, A., & Knyazikhin, Y. (2000). Evaluation of canopy biophysical variable retrieval performances from the accumulation of large swath satellite data. *Agronomie*, *20*, 3–22.

White, M., Thornton, P. E., Running, S. W., & Nemani, R. R. (2000). Parameterization and sensitivity analysis of the BIOME-BGC terrestrial ecosystem model: Net primary production controls. *Earth Interactions*, *4*, 1–85.

Zarco-Tejada, P., Miller, J., Harron, J., Hu, B., Noland, T., Goel, N., et al. (2004). Needle chlorophyll content estimation through model inversion using hyperspectral data from boreal conifer forest canopies. *Remote Sensing of Environment*, *89*, 189–199.